Thin Solid Films 518 (2010) 5694–5699

Contents lists available at ScienceDirect

Thin Solid Films

journal homepage: www.elsevier.com/locate/tsf

Influence of the surface morphology and microstructure on the biological properties of Ti–Si–C–N–O coatings

Cristina Oliveira [a], R. Escobar Galindo [b,d], C. Palacio [c], L. Vázquez [d], A. Espinosa [d], B.G. Almeida [a], M. Henriques [e], S. Calderon V [a], S. Carvalho [a,*]

[a] Departamento de Física, Universidade do Minho, Campus de Azurém, 4800-058 Guimarães, Portugal
[b] Centro de Microanálisis de Materiales, Universidad Autónoma de Madrid, Cantoblanco, 28049, Spain
[c] Departamento de Física Aplicada (CXII), Universidad Autónoma de Madrid, Cantoblanco, 28049, Spain
[d] Instituto de Ciencia de Materiales de Madrid (ICMM-CSIC), Cantoblanco, 28049, Madrid, Spain
[e] IBB-Institute for Biotechnology and Bioengineering, Centre for Biological Engineering, Universidade do Minho, Campus de Gualtar, 4700-057, Portugal

ARTICLE INFO

Available online 10 May 2010

Keywords:
Ti–Si–C–N–O coatings
Thin films
Magnetron sputtering
Structural properties
Microstructural properties
X-Ray Diffraction
Atomic force microscopy
Biocompatibility

ABSTRACT

Detailed structural, microstructural, biofilm formation and cytotoxicity studies were performed on Ti–Si–C–ON hard coatings prepared by DC reactive magnetron sputtering, in order to evaluate the relation among these properties. Compositional analysis showed the existence of two distinct regimens; regime I: high C/Si atomic ratio ($C/Si \geq 1.42$) and intermediate N/Ti atomic ratio; regime II: low C/Si atomic ratio ($C/Si \leq 0.49$) and low N/Ti atomic ratio. The structural analysis revealed that, in regime I, films crystallized in a B1-NaCl crystal structure typical of $TiC_{0.2}N_{0.8}$. In regime II, the decrease of C/Si and increase in silicon concentration led to the formation of Ti–Si–C–ON along with a reduction of grain size in the films. Atomic force microscopy observations showed that the surface morphology of these Ti–Si–C–ON films became smoother when the silicon content increased and the nitrogen content decreased, which is consistent with the formation of nanosized clusters. Concerning biological properties, it was observed that cytotoxicity could be related with the titanium concentration while biofilm formation ability was found to be related with the surface morphology of the films.

1. Introduction

The increasing demand for sustainable products requires the development of new knowledge-based materials with advanced properties. These products are then expected to: last longer, have a better performance, be safe, and be more efficient. These requirements, which maybe seen as a rule of thumb for most known materials, gain particular importance when dealing with applications involving the human body: the so-called biomaterials. Typically these requirements are extremely sensitive to structure variation at the micrometric or nanometric scales and it is important to understand their correlation with the material's microstructure [1]. In fact, this knowledge helps to prevent infections and precocious consuming of the developed biomaterials. Beyond the physical and structural characterizations, the study of the biological properties, in particular biofilm formation and cytotoxicity, has also an important role. Biofilm represents a structured community of bacterial cells embedded in a self-produced polymeric matrix adherent to the artificial surface [2]. Cytotoxicity, on the other hand, characterizes the surface's degree of toxicity to cells.

The purpose of this work is to investigate the feasibility of various Ti–Si–C–ON mechanical hard coatings for applications in medical devices (e.g. for knee and hip joint prostheses as well as for medical instruments such as lithotripters). According to the literature, it is widely accepted that it is possible to achieve superhardness by incorporation of silicon (Si) in titanium nitride (TiN) [3], and a decrease in the Young's modulus is observed by addition of oxygen [4]. Oxygen has always been looked upon as an interesting element in thin film materials, not only because of its high reactivity with most metals, but also due to the changes that it induces in chemical bonding states and, therefore, in the material's electrical, optical and mechanical characteristics [5]. In addition, it has been previously shown that corrosion resistance tends to be slightly improved by oxygen incorporation [6]. Also, recent work on the Ti–Si–C system showed that it is a promising compound due to its particular structure and extraordinary mechanical and tribological properties [7].

Taking this into consideration, the feasibility of coating materials based on Ti, Si, C, O and N will be determined through the correlation between their structural (roughness, chemical composition and phase composition) and biological (biofilm formation ability and cytotoxicity) properties.

* Corresponding author. Tel.: + 351 253 510470; fax: + 351 253 510461.
E-mail address: sandra.carvalho@fisica.uminho.pt (S. Carvalho).

0040-6090/$ – see front matter © 2010 Elsevier B.V. All rights reserved.
doi:10.1016/j.tsf.2010.05.050

2. Materials and methods

The Ti–Si–C–ON samples were deposited by DC reactive magnetron sputtering, in an Ar + (N_2 + O_2) atmosphere, from two opposed high purity (99.6%) rectangular Ti targets (20 × 10 cm^2). One Ti target had Si pellets incrusted (hereafter designated as the TiSi target) and the other had carbon pellets (designated as the TiC target) placed in the preferential eroded zone. The area occupied by the pellets was close to 11 cm^2, in each target. AISI 316L stainless steel (surface area of 2 × 2 cm^2 and mechanically polished until a mirror-like surface finish) and a (100) single crystalline silicon were used as substrate materials. Prior to deposition, the substrates were ultrasonically cleaned during 15 min in propanol and sputter-etched for 20 min in an argon atmosphere. The substrate bias voltage and the temperature were kept constant at −50 V and 200 °C, respectively. A gas atmosphere composed by Ar + (N_2 + O_2) was kept at constant pressure. The base pressure in the chamber was about 10^{-4} Pa and rose to 4.5×10^{-1} Pa during the depositions. Different TiC/TiSi target current combinations were used, being the current density applied to the magnetrons in the range 0 to 10 mA/cm^2, for both targets (see Table 1).

The stoichiometry of the films deposited on both substrates was investigated by means of Rutherford Backscattering Spectrometry (RBS) and Glow Discharge Optical Emission Spectroscopy (GDOES). RBS measurements were performed with a 5 MV HVEE Tandetron [8] using He ions at 3.7 MeV to make use of the resonance of alpha particles with nitrogen at this specific energy. GDOES was carried out using a Jobin Yvon RF GD Profiler equipped with a 4 mm diameter anode and operating at a typical radio frequency discharge pressure of 650 Pa and power of 40 W.

Ball crater tests were used to obtain the thickness of the samples. X-Ray Diffraction (XRD) with a grazing incidence mode (angle of incidence of 1.5°) using a Cu anode (Cu Kα = 1.54 Å) at room temperature was performed on a Siemens D-5000 difractometer, to characterize their structure. The chemical bonding information was obtained by Raman and X-Ray Photoelectron Spectroscopy (XPS). Raman spectra were acquired with a Jobin Yvon HR 460 monochromator, a nitrogen cooled CCD, and the excitation light was the 514.5 nm line of an Ar–Kr laser. The incident and scattered beams were focused using an Olympus microscope. A Kaiser Super-Notch filter was used to suppress the elastic scattered light. XPS spectra were measured using a hemispherical analyzer (SPECS EA-10 Plus). The pass energy was 15 eV giving a constant resolution of 0.9 eV. The Ag $3d_{5/2}$ line at 367.9 eV was used in order to calibrate the binding energies. A twin anode (Mg and Al) X-ray source was operated at a constant power of 300 W using Mg Kα radiation. The samples were sputter-cleaned *in situ* using a broad 3 keV Ar^+ beam for 10 min.

Atomic force microscopy (AFM) observations of the topography of the coating surface were carried out using a Nanoscope IIIa model from Digital Instruments operating in tapping mode. Silicon cantilevers, with a nominal radius of curvature of 10 nm, were used. AFM images over scanning areas of 2 × 2 μm^2 with a resolution of 512 × 512 pixels were obtained The root-mean square (rms) roughness values were calculated over 2 × 2 μm^2 areas for, at least, 5 images.

Before performing the biological assays, samples were sterilized at 121 °C and 1 atm, for 15 min. Biofilms of *Staphylococcus epidermidis* were formed on the coated materials and in well plates with agitation (100 rpm). After 48 h, the total biomass was determined by the crystal violet (CV) staining method [9]. Briefly, 1 ml of CV (1% v/v) was added to each well containing each sample and incubated for 5 min. The wells were then gently washed with sterile ultra-pure water and 1 ml of acetic acid (33% v/v) was added to release and dissolve the stain. The absorbance of the obtained solution was read in triplicate in a microtiter plate reader at 570 nm. Assays were performed in triplicates, in three independent assays.

Cytotoxicity was determined by indirect contact of samples with Fibroblasts 3T3 (CCL-163). Cellular activity was determined by MTS quantification (3-(4,5-dimethylthiazol-2-yl)-5-(3-carboxymethoxyphenyl)-2-(4-sulfophenyl)-2H-tetrazolium, inner salt — Promega CellTiter 96® AQueous Non-Radioactive Cell Proliferation Assay). The samples were placed on wells of a cell culture plate, containing a confluent layer of fibroblasts, at 5% CO_2 and 37 °C. After 24 h of incubation, 1 ml of medium with 20 µL of MTS was added to each well, after the removal of the sample. Then the plate was incubated for 1 h and the absorbance of the resulting solution was read at a wavelength of 540 nm. The percentage of fibroblasts death was determined against cell growth in the absence of the sample (control — 100%). Assays were performed in triplicates and in three independent assays. The results of biofilm formation and % of cell death obtained for the different averages were compared using a *t*-Student test with a confidence level of 95%.

3. Results and discussion

3.1. Chemical composition

The as-deposited sample thickness, measured by ball cratering, and their atomic composition determined by RBS and GDOES, as a function of the target's current ratio (I_{Ti-C} stands for the DC current applied to Ti–C target and I_{Ti-Si} corresponds to the DC current applied to Ti–Si target) are given in Table 1. It should be pointed out that there is no significant difference between the results obtained by the two techniques, for both substrates. As expected, a decrease of the carbon content, from 11.01 to 3.9 at.%, and an increase of the silicon content, from 2.84 to 9.6 at.%, are observed when the I_{Ti-C} decreases from 2 to 0 A and I_{Ti-Si} increases from 0.5 to 2 A. Consequently, in the films, the C/Si ratio varies as a function of the applied I_{Ti-C}/I_{Ti-Si}.

N/Ti ratios do not remain constant in the films, changing as a function of the C/Si content. In fact, the N/Ti atomic ratio has a clear and systematic decrease as C/Si decreases. An increase in the deposition rate with a reduction on the C/Si ratio (or the N/Ti ratio) can be observed in Table 1. Usually, this variation is explained by taking into account the occurrence of target poisoning by both reactive gases. However, this cannot be the reason in the present case since the target potentials remained constant during all depositions. Thus, a competition between the removal sputtering rate of both targets must have occurred, being higher at the Ti–Si target. Keeping in mind that the flow of reactive gas is always the same, an increase on the deposition rate for higher DC current applied to the Ti–Si target induces re-sputtering in the substrate, with a selective removal of Si, leading to an increase in Ti content and, consequently, an N deficiency. Furthermore, it is also important to note that although using no power in the Ti–C target, an amount of about 4 at. % of C is found in this sample. This is due to residual cross contamination

Table 1
Chemical composition, deposition parameters and biological properties of the deposited samples.

Ratio C/Si	Ratio N/Ti	I_{Ti-C} (A)	I_{Ti-Si} (A)	Chemical composition					Thickness (µm)	Deposition rate (µm/h)	Abs CV	% Cell death
				Ti (at.%)	C (at.%)	Si (at.%)	O (at.%)	N (at.%)				
3.9	0.94	2	0.5	37.8	11	2.8	12.8	35.6	1.7	1.1	0.23 ± 0.03	3.8 ± 0.5
1.42	0.86	1	1.2	41.9	7.8	5.5	8.8	36	1.8	1.2	0.25 ± 0.05	23.8 ± 2.4
0.49	0.36	0.5	2	56.8	4.8	9.7	8.4	20.3	2.9	2	0.17 ± 0.02	11.6 ± 0.8
0.42	0.29	0	2	60.7	3.8	9.1	8.8	17.6	3.1	2.1	0.17 ± 0.01	10.5 ± 1.4

of the Ti–Si target during the previous co-depositions using the Ti–C and Ti–Si targets.

A deeper analysis of the compositional results allows the possibility to distinguish two distinct regimes of samples. The first regime (regime I) corresponds to films with a high C/Si atomic ratio ($C/Si \geq 1.42$) and an intermediate N/Ti atomic ratio ($N/Ti \geq 0.86$). The films within the second regime (regime II) have a low C/Si atomic ratio ($C/Si \leq 0.49$) and a low N/Ti atomic ratio ($N/Ti \leq 0.36$). The composition results are well correlated with the structural features of the films. The structural difference within each regime that will be evidenced in the following sections, is the main reason for the selection of these two distinct regimes.

3.2. AFM results

In order to understand the evolution of the microstructure, which correlates directly with the morphology, atomic force microscopy (AFM) measurements were performed on the coatings. Fig. 1 shows micrographs of the Ti–Si–C–ON films deposited on stainless steel, with representative 2D AFM images for each regime. As the C/Si and N/Ti atomic ratios decrease the surface morphology displays a slight smoothening. Indeed, the maximum root-mean square (rms) roughness is obtained at regime I for the sample with the highest C/Si ratio ($C/Si = 3.9$) and intermediate N/Ti ratio ($N/Ti = 0.9$) and the minimum is obtained within regime II ($C/Si \leq 0.42$) and low N/Ti ratio ($N/Ti \leq 0.36$). Moreover, associated to smoothening, the surface presents grains with lateral sizes that become progressively smaller with decreasing C/Si and N/Ti ratios. This indicates a progressive reduction of the crystallite (grain) sizes towards the formation of nanosized clusters in the films, as observed from the XRD analysis (see Section 3.3).

The observed variation of surface morphology is due to the variation of the competitive growth of the different phases, resulting from the different deposition parameters, as will be discussed later. It should be pointed out, that the variation of sample roughness suggests a change in film growth from a Stranski–Kratanov type (in regime I) to a more layer by layer mode (in regime II). The first growth mode is characterized by an island-type film formation, which tends to induce increased surface roughness [10].

3.3. Phase formation

Fig. 2 shows the XRD diffraction patterns for the deposited samples on silicon with different C/Si atomic ratios. International Centre for Diffraction Data (ICDD) of α-Ti (ICDD card nr. 44-1294), TiN (ICDD card nr. 38-1420), TiC (ICDD card nr. 01-071-6256), $TiC_{0.2}N_{0.8}$ (ICDD card nr. 01-076-2484),$C_{0.3}N_{0.7}Ti$(ICDD card nr. 00-042-1488), Ti_5Si_3 phase (ICDD card nr. 29-1362), SiN_x (card nr. 9-245), Si_3N_4 (card nr. 33-1160) and Ti_2CN (card nr. 01-071-6059) are also included at the top of Fig. 2. The results revealed that each of the different C/Si and N/Ti atomic ratio regimes corresponds to different structural arrangements. A similar tendency was observed for the coatings deposited on stainless steel. Here, only the results obtained for Si substrate are presented in order to clarify the analysis.

The XRD patterns of samples with high C/Si atomic ratio and intermediate N/Ti ratio (regime I), exhibit a peak at $2\theta = 36.46°$ that can

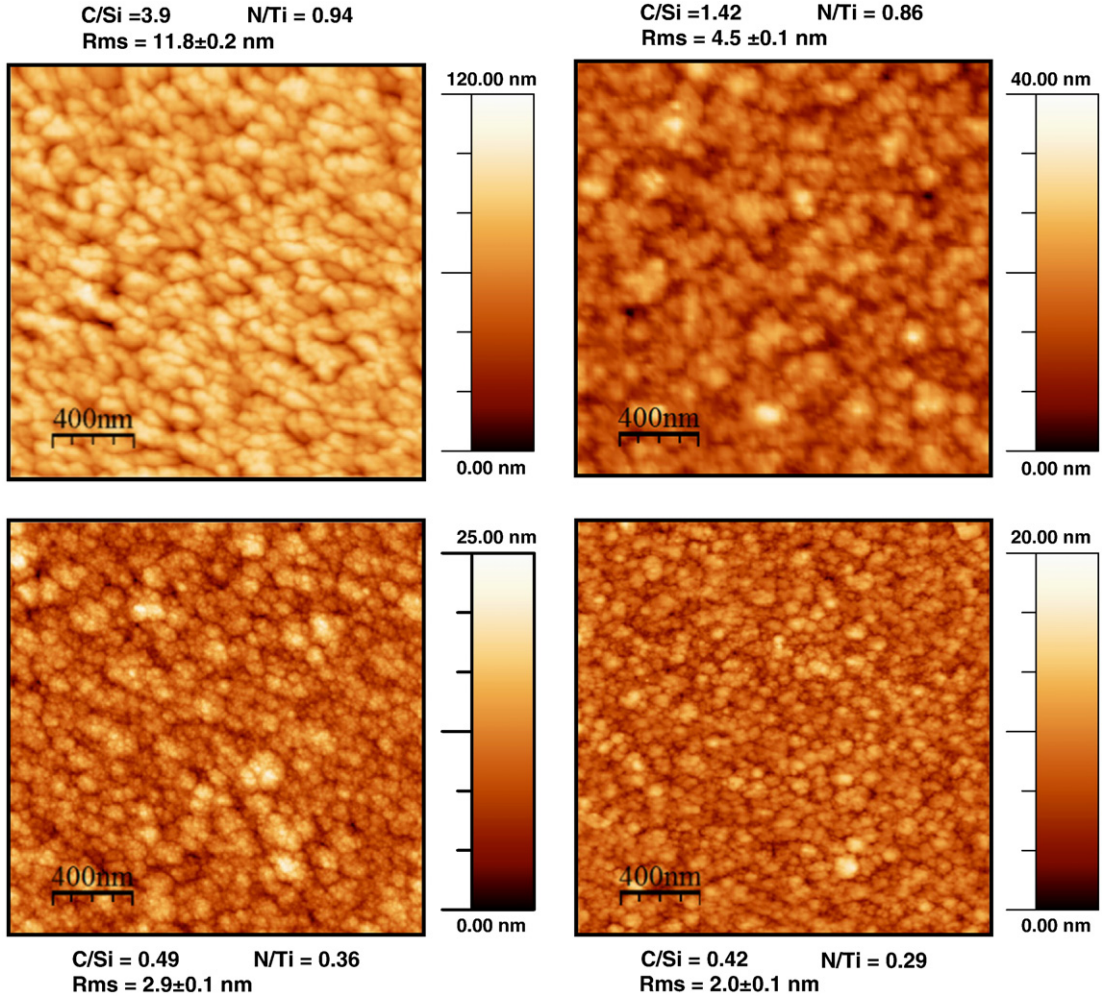

Fig. 1. Surface morphology and roughness of the Ti–Si–C–ON coatings deposited by DC reactive magnetron sputtering. Also presented are the representative 2D AFM images with four different C/Si ratios.

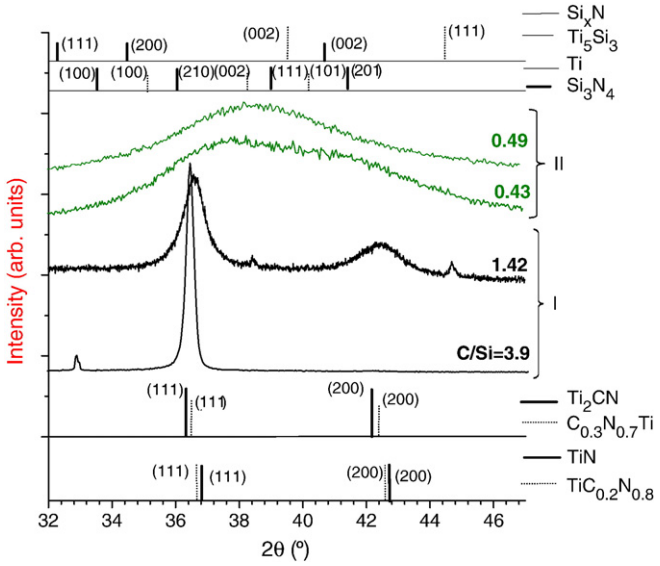

Fig. 2. XRD patterns of the Ti–Si–C–ON coatings deposited by DC reactive magnetron sputtering on silicon, with different C/Si ratios.

be attributed to a B1-NaCl-like crystal structure, typical of $C_{0.3}N_{0.7}Ti$. For the C/Si ratio (C/Si = 1.42), the films crystallize also in a B1-NaCl crystal structure, typical of $TiC_{0.2}N_{0.8}$. This sample shows an additional diffraction peak, at 44.6°, which can be assigned to the (101) direction of $Ti_2C_{0.06}$ with a hexagonal structure, in accordance with the ICDD card number 051-0628 [11]. The presence of these peaks can be explained by the decrease of carbon content.

On the other hand, the silicon could be in grain boundaries, forming a SiN_x amorphous phase. In fact, due to the low deposition rate, the surface mobility should be enough to ensure the segregation of the Si atoms and consequent formation of an amorphous phase (SiN_x). For the sample with C/Si = 1.42 the segregated Si can be enough to nucleate and develop SiN_x phases that in turn form a layer on the growth surface covering the Ti(C,N) nanocrystallites. This hinders their growth [12], leading to smaller crystallite sizes and broader diffraction peaks, as observed on the measured diffraction spectra.

For regime II, the much higher lattice disorder is attributed to a higher deposition rate and to the lower N/Ti and C/Si atomic ratios. In this regime the structure is characterized by a very broad peak in the range 30 to 50° which is not enough to identify the structure. However, there are fcc phases that have the main peaks close to these values, as for example: α-Ti, Ti_2CN, SiN_x, Ti_5Si_3 and Si_3N_4 phases. In fact, an increase in the deposition rate, observed in regime II, without a significant increase in the density bias current at the substrate, induces a decrease in the ion to atom flux ratio and consequently to a decrease of the adatom surface mobility. These conditions do not provide the necessary atomic surface mobility for the Si segregation in the growing film and, thus, very small, nanometre sized, clusters can be formed on the films. By using the width of the peak at ~38° and the Scherrer equation [13], the grain size of the sample with lower C/Si (and lower N/Ti) is estimated to be ~3 nm, consistent with the AFM results previously discussed.

On the other hand, the decrease in the C/Si ratio, with the consequent increase of silicon concentration, along with the increasing number of N-vacancies that can be progressively filled by silicon atoms (due to the decreasing N/Ti), leads to the formation of Ti–Si–C–ON.

3.4. Raman and XPS analysis

In order to further understand the structural and chemical properties of the films, Raman and XPS studies were performed on the Ti–Si–C–ON samples, deposited on silicon substrates, with different C/Si and N/Ti atomic ratios.

Fig. 3 shows the Raman spectra of deposited Ti–Si–C–ON samples. The absence of sharp and well defined peaks is consistent with the presence of a small grain sized structure on the polycrystalline films. Fig. 4 shows Ti2p, Si2p, C1s, N1s and O1s core level spectra of the deposited Ti–Si–C–ON films.

For the samples with C/Si ≥ 1.42 and intermediate N/Ti atomic ratio (regime I), Constable et al. [14] stated that the dispersion curves lead to a group of 'lines' (bands) due to acoustic phonon modes in the 150–300 cm^{-1} region (longitudinal acoustical (LA) and transverse acoustical (TA) modes) and another set of lines due to optic modes in the 400–650 cm^{-1} region (longitudinal optical (LO) and transverse optical (TO) modes). Thus, the four weak and broad bands in Raman spectra, centred about 300, 332, 550 and 568 cm^{-1} can be associated to acoustic (LA/TA) and optical (LO/TO) phonon modes of TiN and TiCN [14,15]. These modes can be associated with the presence of the Ti(C,N) phase, consistent with XRD results. On the XPS analysis, the Ti2p spectra (Fig. 4a) can be simulated using two doublet (Ti2p3/2 and Ti2p1/2 separated by 5.8 eV) contributions ascribed to Ti–N (electron binding energies at 455 and 460.8 eV) and Ti–C (454.5 eV and 460.3 eV) bonds, according to the literature [15–17]. In order to quantify separately the individual contribution of those two phases a complete deconvolution of the spectra should be performed. Therefore, in the following discussion we will refer to them as a Ti–C–N phase. However, these binding energies for titanium are consistent with the C–Ti and N–Ti bonds observed at the C1s (282 eV) and N1s (397 eV) XPS spectra of Fig. 4c and e, respectively. Furthermore, there is evidence of graphitic C–C bonds at 284.5 eV and the presence of C–N bonds with carbon atoms hybridized sp^2 with binding energies of approximately 286.1 eV [18], cannot be discarded. For this same regime, the Si2p XPS spectrum (Fig. 4b) shows a major contribution at 102 eV attributed to Si–N bonds [18] that can be associated to an amorphous SiN_x phase. However, this asymmetric broad peak suggests the presence of at least other two minor contributions as Si–O (103 eV) and Si–C–N (101.4 eV) bonds [18]. Within the O1s region it is evident the appearance of a wide peak (FHWM > 3 eV) centred at 531.2 eV. This binding energy lies between the reported values for O–Ti (529.6 eV) and O–Si (532.7), suggesting the formation of titanium silicates. The Raman band around 720 cm^{-1} that starts to appear in the sample with C/Si = 1.42 (see Fig. 3), is associated to the presence of C–N bonds in the films [19,20]. The Si–O band appearing at ~1100 cm^{-1} is due to the asymmetric stretching vibration of Si–O bonds [21].

For regime II (C/Si ≤ 0.43 (low ratio) and low N/Ti ratio), in addition to the Ti–C–N phase, an extra contribution located at 454.4 eV has to be included to the analysis of the Ti2p XPS spectra. This is attributed to Ti–Si bonds [20], suggesting that Si may be incorporated into the Ti(C,N) films during deposition, forming a Ti–Si–(C,N) solid solution. Regarding Si2p

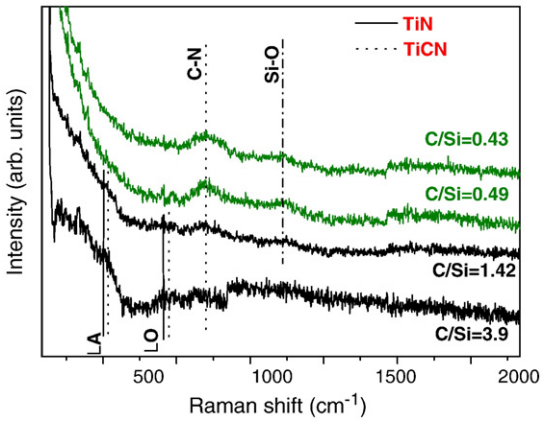

Fig. 3. Raman spectra of the Ti–Si–C–ON coatings deposited by DC reactive magnetron sputtering on silicon, with different C/Si ratios.

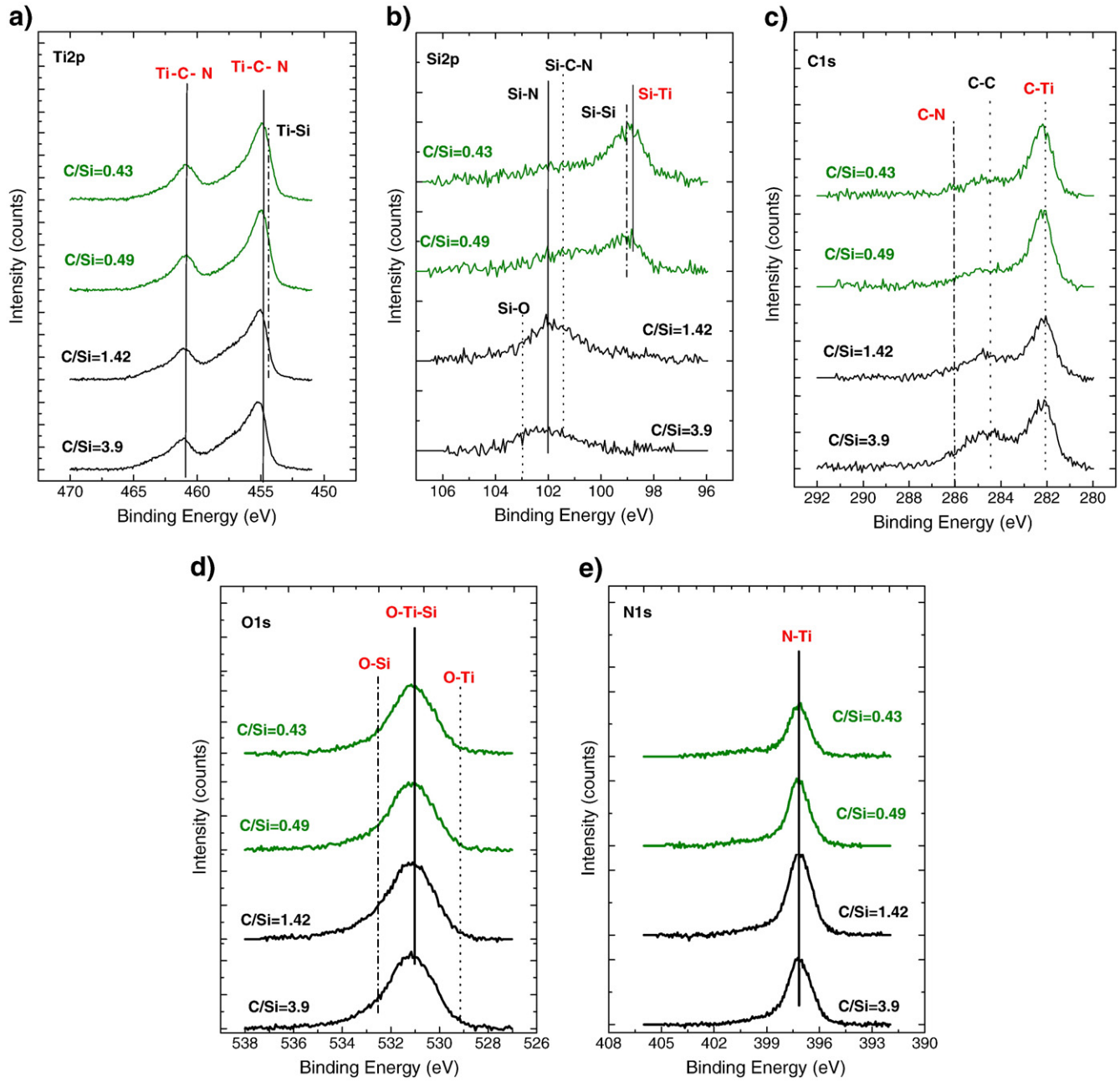

Fig. 4. XPS spectra of a) Ti2p, b) Si2p, c) C1s, d) O1s and e) N1s core levels of the Ti–Si–C–ON coatings deposited by DC reactive magnetron sputtering on silicon, with different C/Si ratios.

spectra, the main difference with samples from regime I is the clear reduction of the Si–N and Si–C–N contribution and the appearance of a major peak at 99 eV. In the literature this contribution is typically ascribed to metal Si bonds [18], although other authors do not discard the formation of Si–Ti bonds as titanium silicides can also be formed [22–24]. In the C1s and N2p spectra, as expected, there is a decrease of the graphitic C–C and the N–Ti contributions with the reduction of the C/Si and N/Ti ratio, respectively. In the Raman spectra it is possible to observe the increase of the band around 720 cm^{-1}, which is due to an increasing number of C–N bonds with decreasing C/Si and N/Ti atomic ratios. These bonds can be formed in the grain boundaries of the nanosized clusters, with carbon bonding to neighbouring nitrogen, or can be due to the presence of carbon in lattice sites adjacent to nitrogen, which is gradually very low to occupy all the available places as it would normally do in the TiN.

3.5. Biological behaviour

Concerning the biological behaviour of the coated samples (Table 1), it is possible to see that there is no systematic trend of the biofilm biomass (Abs CV) or cytotoxicity (% cell death) evolution with the C/Si and N/Ti atomic ratios. However, it is interesting to note that samples from regime II (lower C/Si and N/Ti ratios) present similar behaviour regarding both biological properties.

Concerning biofilm formation ability, samples from regime I present higher values of biomass than samples from regime II ($p<0.05$). Several factors have been found to be related with biofilm formation ability, namely the surface morphology and roughness [25,26] as well as surface chemical composition [27]. From Fig. 1 it is possible to observe that samples from regimen I present higher roughness corresponding to a more heterogeneous surface, which may allow more bacteria to adhere

and consequently to develop more biofilm biomass. Moreover, it is possible to observe (Table 1) that a reduction of C/Si and N/Ti content, along with the decreasing ratio of the non-metallic (C,N,O) to metallic (Ti,Si) elements, leads to a decrease in the cell ability for biofilm formation.

The differences in cytotoxicity (Table 1) found between samples from regime I and regime II ($p<0.05$) cannot be explained alone by the results obtained on surface microstructure characterization. Samples from regime I present extremes of cytotoxicity, having the higher and the lower percentage of cell death from the group studied. On the other hand, samples from regime II present similar and somewhat lower values of cytotoxicity. It is known that titanium, as well as its compounds with nitrogen and oxygen, have excellent biocompatibility. This is due to the moderate surface charge present under biological conditions and the similarity of its dielectric constant to that of water [28]. Additionally, nanosized clusters of silicon (as observed on the X-ray results) tend to have increased cytotoxicity as compared with their micron-sized counterparts [29]. Here, samples from regime II present a high amount of titanium on their composition (bigger than 55%) which can account for the lower observed cytotoxicity. Thus, for biomedical purposes, samples with i) low values of C/Si and N/Ti (that presented low roughness) and ii) high concentration of titanium should be selected since they present low biofilm formation and also low cytotoxicity. It is interesting to note that similar coatings, deposited with different preparation conditions, but at the same low N/Ti ratio [11], were also less prone to *S. epidermidis* colonization.

4. Conclusions

Ti–Si–C–ON films were synthesized by unbalanced DC magnetron sputtering and their structural and biological properties were characterized. From the composition results, the variation of the C/Si ratio on the deposited films was obtained. The N/Ti atomic ratio had a systematic reduction with decreasing C/Si. Taking into account the different elemental compositions and structures, two different regimes could be considered: regime I: high C/Si atomic ratio ($C/Si \geq 1.42$) and intermediate N/Ti atomic ratio; and regime II: low C/Si atomic ratio ($C/Si \leq 0.49$) and low N/Ti atomic ratio. AFM observations showed that the surface morphology of these Ti–Si–C–ON films became smoother with increasing silicon and lower nitrogen content, consistent with the formation of nanosized clusters with the reduction of the C/Si and N/Ti ratios.

In regime I, the films crystallized in a B1-NaCl crystal structure typical of $TiC_{0.2}N_{0.8}$ and the silicon was in grain boundaries in one SiN_x amorphous phase. Samples from regime I had higher roughness, that induced higher biofilm formation, and extremes in cytotoxicity.

In regime II, the decrease in C/Si with the consequent increase in silicon concentration, along with the increase in the number of N-vacancies, leads to the formation of Ti–Si–C–ON. They showed similar and somewhat lower cytotoxicities, due to the higher Ti content in the films, and lower biofilm formation.

Consequently, for biomedical purposes, samples with high Ti concentrations and with low values of C/Si and N/Ti (regime II), which presented lower roughness, should be selected, since they present low biofilm formation ability and also low cytotoxicity.

Acknowledgments

The authors are grateful to Dr. Alicia Andrés, Instituto de Ciencia de Materiales de Madrid (ICMM-CSIC), for her assistance in carrying out the Raman spectroscopic analysis. The project was financially supported by the CRUP Institution (project "Acção Nº E-1007/08"), and the Spanish Ministry of Science and Innovation (projects FUNCOAT CSD2008-00023 and HP2007-0116).

References

[1] N.M. Alves, C.S. Arroyo, M.A.R. Perez, R.L. Reis, J.F. Mano, Acta Biomater. 3 (2007) 69.
[2] S. Roveta, A. Marchese, G.C. Schito, Int. J. Antimicrob. Agents 31 (2008) 321.
[3] S. Veprěk, A. Nioderhofer, K. Moto, Surf. Coat. Technol. 133 (134) (2000) 152.
[4] F. Vaz, P. Cerqueira, L. Rebouta, S.M.C. Nascimento, E. Alves, P.H. Goudeau, J.P. Rivière, Surf. Coat. Technol. 174 (175) (2003) 197.
[5] A.C. Fernandes, P. Carvalho, F. Vaz, S.L. Méndez, A.V. Machado, N.M.G. Parreira, J.F. Pierson, N. Martin, Thin Solid Films 515 (2006) 866.
[6] E. Ariza, L.A. Rocha, F. Vaz, L. Cunha, S.C. Ferreira, P. Carvalho, L. Rebouta, E. Alves, P.H. Goudeau, J.P. Rivière, Thin Solid Films 469 (470) (2004) 274.
[7] C. Lopes, N.M.G. Parreira, S. Carvalho, A. Cavaleiro, J.P. Rivière, E.L. Bourhis, F. Vaz, Surf. Coat. Technol. 201 (2007) 7180.
[8] A. Climent-Font, F. Pászti, G. Garcia, M.T.F. Jiménez, F. Agulló, Nucl. Instrum. Methods. Phys. Res. Sect. B 219 (220) (2004) 400.
[9] M. Henriques, J. Azeredo, R. Oliveira, Br. J. Biomed. Sci. 63 (2006) 5.
[10] M. Ohring, The Materials Science of Thin Films, Academic Press Inc., San Diego, 1992.
[11] C. Oliveira, L. Gonçalves, B.G. Almeida, C.J. Tavares, S. Carvalho, F. Vaz, R. Escobar Galindo, M. Henriques, M. Susano, R. Oliveira, Surf. Coat. Technol. 203 (2008) 490.
[12] S. Carvalho, E. Ribeiro, L. Rebouta, J. Pacaud, Ph. Goudeau, P.O. Renault, J.P. Rivière, C.J. Tavares, Surf. Coat. Technol. 172 (2003) 109.
[13] B.D. Cullity, S.R. Stock, Elements of X-Ray Diffraction, Prentice Hall, Reading, MA, 2001.
[14] C.P. Constable, J. Yarwood, W.D. Munz, Surf. Coat. Technol. 116 (119) (1999) 155.
[15] D. Pilloud, J.F. Pierson, M.C.M. Lucas, A. Cavaleiro, Surf. Coat. Technol. 202 (2008) 2413.
[16] X. Song, D. Gopireddy, C.G. Takoudis, Thin Solid Films 516 (2008) 6330.
[17] J. Alami, P. Eklund, J. Emmerlich, O. Wilhelmsson, U. Jansson, H. Högberg, L. Hultman, U. Helmersson, Thin Solid Films 515 (2006) 1731.
[18] B. Mitu, G. Dinescu, M. Dinescu, A. Ferrari, M. Balucani, G. Lamedica, Thin Solid Films 383 (2001) 230.
[19] E.J. Liang, J.W. Zhang, J. Leme, C. Moura, L. Cunha, Thin Solid Films 469 (470) (2004) 410.
[20] J.S. Colligon, V. Vishnyakov, R. Valizadeh, S.E. Donnelly, S. Kumashiro, Thin Solid Films 485 (2005) 148.
[21] B.G. Almeida, A. Pietka, P. Caldelas, J.A. Mendes, J.L. Ribeiro, Thin Solid Films 513 (2006) 275.
[22] J. Perez-Mariano, K.-H. Lau, A. Sanjurjo, J. Caro, D. Casellas, C. Colominas, Surf. Coat. Technol 201 (2006) 2217.
[23] F. Zhaoa, X. Cuia, B. Wang, J.G. Hou, Appl. Surf. Sci. 253 (2006) 2785.
[24] S. Veprěk, A. Niederhofer, K. Moto, T. Bolom, H.-D. Männling, P. Nesladek, G. Dollinger, A. Bergmaier, Surf. Coat. Technol. 133–134 (2000) 152.
[25] H. Tang, T. Cao, X. Liang, A. Wang, S.O. Salley, J. McAllister II, K.Y. Simon Ng, J. Biomed. Mater. Res. A 88A (2009) 454.
[26] I. Apilanez, A. Gutierrez, M. Diaz, Biores. Tech. 66 (1998) 225.
[27] B.L. Gabriel, J. Gold, A.G. Gristina, B. Kasemo, J. Lausmaa, C. Harrer, Q.N. Myrvik, Biomaterials 15 (1994) 628.
[28] D.M. Brunette, P. Tengvall, M. Textor, P. Thomsen, Titanium in Medicine: Material Science, Surface Science, Engineering, Biological Responses and Medical Applications, Springer, New York, 2001, p. 1019.
[29] J. Choi, Q. Zhang, V. Reip, N.S. Wang, M.E. Stratmeyer, V.M. Hitchins, P.L. Goering, J. Appl. Toxicol. 29 (2009) 52.